Structural and Electrical Properties of Zn1-xCrxO NTCR Nanoceramics Synthesized by High Energy Ball Milling

Bikram Keshari Das
Kalinga Institute of Social Sciences(KISS),Deemed to be University,Bhubaneswar

Tanushree Das
Kalinga Institute of Social Sciences

Kajal Parashar
KIITS University: Kalinga Institute of Industrial Technology

S.K.S Parashar (sksparashar@yahoo.com)
KIIT University https://orcid.org/0000-0001-8739-7765

Rajeev Kumar
IISC Bangalore: Indian Institute of Science

Anupama . A. V
IISC Bangalore: Indian Institute of Science

Balaram Sahoo
IISC Bangalore: Indian Institute of Science

Research Article

Keywords: Cr doped ZnO, HEBM, Rietveld refinement, SEM, NTCR behaviour

Posted Date: February 23rd, 2021

DOI: https://doi.org/10.21203/rs.3.rs-221973/v1

Structural and electrical properties of $Zn_{1-x}Cr_xO$ NTCR nanoceramics synthesized by high energy ball milling

Bikram Keshari Das[1*], Tanushree Das[1], Kajal Parashar[2], S. K. S. Parashar[2,*], Rajeev Kumar[3], Anupama A. V.[3], Balaram Sahoo[3]

[1] *Department of Chemistry, Nano centre of Excellence, Kalinga Institute of Social Sciences (KISS) Deemed to be University, Bhubaneswar-751024, Odisha, India*

[2] *School of Applied Sciences, Nano Sensor Lab, KIIT University, Bhubaneswar-751024, Odisha, India*

[3] *Materials Research Centre, Indian Institute of Science, Bangalore-560012, India*

Abstract

Cr doped ZnO (x = 0-0.04) nanoceramics was successfully synthesized by high energy ball milling (HEBM) technique. The structural and electrical properties of the synthesized sample has been studied in detail. The doping of Cr into ZnO has been verified by X-ray diffraction (XRD) and also from the variation in structural parameters. Rietveld refinement XRD pattern of calcined sample showed the hexagonal wurtzite structure and it did not induce impurity phases. From the XRD, it has been confirm that maximum result confirms that up to 4 atomic% of Cr can be doped into ZnO. The strain of the sample reduced with increase in particle size. After sintering, there is a growth of particle size of Cr doped ZnO sample. The impedance spectroscopy data shows a single semicircle in the high frequency region corresponding to the bulk properties of the nanoceramic sample. The decrease in real part of the impedance with temperature suggests the NTCR behavior of the sample in the temperature range of 300-500 ºC. The temperature dependent relaxation phenomena are also observed for the synthesized ceramic sample at high temperature. Distributed relaxation time suggests that the relaxation in the synthesized samples is of non-Debye type. The equivalent electrical circuit of the semicircular pattern in the impedance spectrum of ZnO and $Zn_{1-x}Cr_xO$ nanoceramics sample is a parallel combination of bulk resistance (R_b) and bulk capacitance (C_b).

Keywords: Cr doped ZnO; HEBM; Rietveld refinement; SEM; NTCR behaviour.

**Corresponding author:* S. K. S. Parashar (sksparashar@yahoo.com)
Bikram Keshari Das (bikram.das@kiss.ac.in)

1 Introduction

Temperature sensors are used in domestic and industrial sector, laboratory and medical processes to regulate the temperature. The electrical behaviour of NTC ceramic depends on factors such as purity, composition, cation distribution [1]. The distribution of cation and oxygen parameter (u), gives information to build up physical properties for application in industry [2]. Nano metal oxide has paying attention of scientific community because of their unique properties like electronic properties, optical properties and large surface to volume ratio. The properties of a materials depend on particle size, crystalline structure, their surface conditions and shape [3]. Different behaviour of metal oxides such as ZnO, In_2O_3, CdO, CuO and SnO_2 have been extensively investigated in doped and undoped form[4-6]. ZnO is an important semiconductor material among different transition metal oxides[7], it has a with wide band gap of ~3.37 eV, large exciton binding energy of ~60 meV having hexagonal wurtzite structure and belong to the space group $P6_3mc$ (C_6v) [8]. Because of its unique properties like non-toxic nature, abundance in nature, low cost, suitability for doping, high thermal and chemical stability and is an important semiconductor materials [9]. ZnO has versatile applications like UV photodetectors [10] gas sensors [11], solar cells [12], spintronics [13] luminescent materials [14], piezoelectric devices [15], light emitting devices [16], Thermistor [17] and cancer treatment [18]. Optical, electrical and other material properties of ZnO can be enhanced and control for its practical applications by doping with selective elements [19]. From the literature, it is found that doping with metal ions makes suitable for specific needs [7]. Several synthesis method has been used to synthesis doped and undoped ZnO nanoparticles such as sol-gel [20], solid state [21], hydrothermal [22] ball milling [23], microwave method [24], sonochemical method [25] etc.

Among these methods, ball milling is superior one because it reduces the phase transition temperature, sintering temperature, increases the particle reactivity. Particle size can be easily decreased to nano scale level and also low temperature solubility limit can be extended [26]. The sintering temperature is important in controlling the intrinsic defects in ZnO and also the properties of the samples [27].

By doping zinc oxide with different transition metals (TM), [28-31] or rare earth (RE) metals properties like electrical, Optical, and magnetic can be changed [32-35].This can be achieved by modifying the electronic structure and band gap of ZnO [36,37] making it appropriate for various applications. Physical properties can be modified by doping ZnO with metal ions like Cd^{2+}, Cu^{2+}, Ni^{2+}, Cr^{3+} and Mn^{2+} for reasonable applications. Chromium has been utilized to upgrade the optical, electrical, magnetic and luminescent behaviour of ZnO [38]. By doping ZnO with different metals like Ni [17], Sr [20], Ca [39], Mn [40], La [41] etc. into ZnO shows NTCR behaviour which is very much

suitable for thermistor application. Among different phases of chromium oxide, under normal conditions Cr_2O_3 is the most stable phase. Therefore conduction properties of ZnO can be modified by Cr doping [7]. As the ionic radius of Cr is very close to that of Zn^{2+}, Cr^{3+} can easily enter into ZnO crystal lattice [42].

The structural and electrical behaviour of oxides can be correlated by complex impedance spectroscopy (CIS) in a broad range of frequencies and also to study their temperature and frequency dependent phenomena [43]. The ac conduction mechanism in amorphous semiconductors can be described by Correlated Barrier Hopping (CBH), Quantum Mechanical Tunneling (QMT) [44], and Hoping over a Barrier [45-47].

Although there are few reports available for ac conductivity study of Cr doped ZnO, a detailed investigation is not done. In this communication, we have presented the study on the structural, morphological and NTCR behaviour of Cr doped ZnO nanoceramics in details. The impedance studies of Cr-ZnO pellets is also carried out for a clear understanding of the suitability of Cr doped ZnO nanoceramics for thermistor application.

2 Experimental details

HEBM technique is used to synthesize Cr doped ZnO ($Zn_{1-x}Cr_xO$ with x = 0 - 0.04) nano-crystalline samples. Calculated quantity of ZnO and Cr_2O_3 has been milled for 10h in a high energy ball mill (PM400 Retsch) in dry milling conditions having ball to powder weight ratio 10:1 with a speed of 300 rpm. Milling parameters like rotation speed, time of milling etc. important role for synthesis of ZnO nanoparticles [48]. The milling process was stopped for 30 min after every 1h of milling. Because of the kinetic energy of grinding medium heat generated during milling and the milling process is exothermic [49]. The milled sample was calcinated at 900 °C for 2h with a heating rate of 2 ºC/min. Then the calcined powder mixed thoroughly with a small amount of PVA for making pellet. The pelletization was done using a hydraulic press at a pressure of 500 Mpa and sintered at 1000 ºC for 2h. Silver paste was applied on the surface of the pellets and dried at 700 ºC for 15 minutes, to make conductor. The structure of the ball milled calcined powder was determined by XRD D8 Advance, Bruker and field emission scanning electron microscopy (FESEM, Carl Zeiss NTS Ltd, UK). By using the "FullProf" program rietveld refinement of the XRD patterns was carried out [50] to quantify different structural parameter. The electrical behavior of the samples were studied using Impedance analyzer (Hioki LCR Hi-tester-3532-50) in a frequency range of 100 Hz –1 MHz and

in a temperature range of 300 °C to 500 °C. The schematic representation of material synthesis experimental process is given in Figure 1.

3 Results and Discussion

3.1. X-ray diffraction

3.1.1 Structural parameters analysis

Figure 2(a) illustrates the XRD pattern of the 10h ball milled $Zn_{1-x}Cr_xO$ samples with different Cr concentration and Figure 2(b) of 10h milled and calcined at 900 ºC samples. All the XRD peaks are matched to wurtzite structure of zinc oxide with a space group $P6_3mc$ and are in good agreement with JCPDS data card 36-1451. It was also found that the peak broadening increases with the concentration of Cr. No supplementary peak associated to Cr_2O_3 or impurity was shown in the XRD patterns of synthesized samples (10h milled) up to 3 atomic% Cr doping. But in case of x = 0.04 only some extra peaks associated to Cr_2O_3 were found at 2θ = 33.71, 50.16 and 54.91for x = 0.04 in case of 10h ball milled sample (Figure 2 (a)), which suggests that Cr^{3+} is replaced by Zn^{2+} in the ZnO crystal lattice for x = 0.01- 0.03 after milling the mixture for 10 h but for x = 0.04 precipitation of Cr_2O_3 was observed. The XRD pattern of calcined sample (900 ºC, 2 h) (Figure 2(b)) confirms that the samples up to 4 atomic % (x = 0.04) of Cr retains their structure intact. It indicates when the sample is calcined at the diffused particle when calcined at 900 ºC the substituted Cr^{3+} ion in the Zn^{2+} ion positions in ZnO lattice up to x= 0.04 which shows the single phase $Zn_{1-x}Cr_xO$ material and no precipitation of Cr_2O_3 was observed. Thus there is no impurity within range of XRD. Therefore, we believe that upto 4% of Cr (x = 0.04) doping is lower than the solubility limit of Cr ion in ZnO lattice by high energy ball milling. More than 4% of Cr doping in ZnO was reported by sol gel method and by a number of researchers[51–53]. K. Sebayang et al. reported more than 3.5% of Cr doping by solid state reaction [54]. It is also noticed that upon calcination the peak intensity increased and FWHM decreased which indicates the crystallinity of the $Zn_{1-x}Cr_xO$ sample increased after calcination[55].

The structural parameters are obtaind from the Rietveld refinement of the XRD patterns of 10h ball milled $Zn_{1-x}Cr_xO$ nanoceramics ((Figure 3(a-f)). It has been observed from Figure 3(a) there is no significant modification in the value of lattice parameter (a and c) due to Cr doping. But a closer study indicates slight increase in the value of both a and c after Cr doping which can be due to the lattice distortion cause due to doping. But it decreases with increases in Cr concentration. This result is consistent with the reported observation [52,53,56,57] . The c/a ratio of ZnO is not much changed by Cr doping while the volume of unit cell reduces slowly with increase in Cr concentration (Figure 3(b)). The value of c/a = 1.60 shows that the hexagonal structure of pure ZnO is not distressed due to Cr doping. The crystallite size and strain was determined by using Scherer equation and W-H method.

The variation of crystallite size and strain with increase in Cr concentration were illustrated in Figure 3(c). It was observed that the crystallite size reduces with increases in Cr concentration in ZnO. This variation of crystallite size is as a result of the substitution of Cr ion in ZnO lattice [52].

The reduction in size may be due to lattice distortion of the ZnO crystal structure due to incorporation of smaller size Cr atom into ZnO lattice [58]. Similar result is also reported by a number of researchers [57,59-61] The lattice strain was increased after Cr doping but by increasing the Cr concentration it was found to be decreased. The result is quite similar as observed by Santi Septiani et al.[56]. Figure 3(d) shows the variation of specific surface area and u-parameter with Cr concentration. The specific surface area (S) was computed by the relation

$$S = \frac{6x10^3}{Dp.\rho} \quad (1)$$

Where S = specific surface area, Dp = size of the particle (nm), ρ = density of ZnO (5.606gm/cm^3).

The specific surface area of Cr doped ZnO shows larger value upto 2% of Cr doping than pure ZnO which is slightly decreases for 3 and 4% of doping. This large value of S shows that sample is more reactive [62].

The u parameter was calculated by using the formula

$$u=\frac{1}{3}\left(\frac{a^2}{c^2}\right)+\frac{1}{4} \quad (2)$$

Slight increase in the value of u-parameter also observed (Figure 3(d)). The change in Zn-O bond length due to doping is calculated using relation

$$L = \sqrt{\frac{a^3}{3}+\left(\frac{1}{2}-u\right)^2 c^2} \quad (3)$$

Where a and c are lattice parameter and u is the oxygen positional parameter. The effect Cr doping on the variation of bond length Zn-O is shown in Figure 3(e). A very small variation of bond length with increase in Cr doping was observed which confirms replacement of ion [63]. Because of the variation in bond length lattice deformation takes place. The lattice distortion degree was calculated by the relation 4.

$$R = \frac{2a\left(\frac{2}{3}\right)^{\frac{1}{2}}}{c} \quad (4)$$

In our case, the lattice parameter (a and c) and Zn-O bond length was found to be decreased with increasing the Cr concentration, which confirms the reduction of crystallite size also the unit cell volume and applicable modification in micro strain .

The average value of δ was calculated by using the relation

$$\delta = \frac{15\beta \cos\theta}{4\,a\,D} \quad (5)$$

By taking first three major planes (100), (002) and (101) are shown in Figure 3(f). It was found that the value of dislocation density (δ) for x = 0.01 doped ZnO is lower than pure ZnO which increases with rise in Cr concentration. The highest value of dislocation density was observed for x = 0.04, indicates the highest hardness among all the samples [64].

3.2 Morphological study by FESEM

The surface morphology of all samples was studied by FESEM. Figure 4(i) illustrates the FESEM pattern of 10h milled undoped and Cr doped ZnO nanoceramics. All compositions exhibit spherical shape with diverse particle sizes. From these pictures it is seen that the particle size reduces with increase of Cr concentration from x = 0 to 0.03 but for x = 0.04, there is a start of agglomeration of the particles forming bigger particles. The elemental composition of all synthesized sample are obtained from EDX and are shown in Figure 4(ii). From Figure ((ii) (a)) it is obvious that the sample contains only Zn & O where as other sample consists of Zn, Cr and O. Presence of any other impurity was not found in the sample, which indicates the purity of the synthesized sample, again the intensity of Cr increases with increasing Cr incorporation in ZnO lattice. So this measurement confirms the presence of Cr in the Cr doped ZnO samples.

3.3 Impedance (Z*) Analysis

The electrical behaviour of all the synthesized material was carried out by Complex Impedance spectroscopy (CIS) in the frequency range 100 Hz - 1 MHz. The output response of such measurement in a complex plot shows in the pattern of a sequence of semicircles, which helps to split the contribution of grain boundary and bulk. The complex impedance of a system can be described as [65]:

$$Z^* = Z' + \mathrm{j}\,Z'' \quad (6)$$

where $Z' = Z\cos\theta$ and $Z'' = Z\sin\theta$.

Similarly Figure 5(x = 0 - 0.04) illustrates the variation of real part of impedance (Z′) with frequency at temperature range of 300-500 °C for $Zn_{1-x}Cr_xO$ nanoceramics sintered at 1000 °C with different concentration of x. From the figure it was found that the magnitude of Z′ (i.e resistance) reduces with rise in temperature and frequency for all samples which indicate the chances of increase in ac conductivity with temperature and frequency [66]. Figure 5(f) shows the variation of Z′ with the Cr concentration at a particular temperature and frequency (300 ºC and 20 kHz). It was observed that with Cr doping the impedance (Z′) becomes higher which increases linearly with raise in Cr concentration.

The increase of Z′ with increasing Cr concentration in ZnO at 300 ºC for all Cr doped samples shows a decrease in the value of ac conductivity with increase in concentration. The decrease in degree of Z′ on raise in temperature shows their NTCR behavior in the studied temperature and frequency range. Again at low frequency and temperature region the value of Z′ is high which may be because of the polarization in the samples. Relaxation process in the materials was observed in the low frequency range [67]. In the temperature range of 300-500 °C $Zn_{1-x}Cr_xO$ nanoceramics shows NTCR behaviour which suggests that, the material can be a suitable candidate for NTCR thermistor applications. The variation of imaginary part of impedance (Z") with frequency at different temperature for $Zn_{1-x}Cr_xO$ samples with different concentration of Cr was shown in Figure 6. The effect of doping is observed from the variation in the magnitude of Z", peak expansion and asymmetry. At higher temperature each curve exhibit peak. A single peak (Z''_{max}) which is temperature dependent is seen for all the samples. The peak shifts towards higher frequencies as the temperature is increased and a broadening observed with the decrease in peak height. This broadening suggest the temperature dependent relaxation phenomena in the material [68]. The relaxation phenomena in the material may be due to the presence of immobile species at low temperature and defect at high temperature[55]. The variation of the peak position and height with concentration of Cr doping was shown in Figure 6(f). The Cr shifts peak frequency to the higher value and it increases linearly with increase in Cr concentration up to x = 0.04.

Figure 7 shows the cole - cole plot of $Zn_{1-x}Cr_xO$ nanoceramics. The observed semicircular arc have their centers laying off the real axis indicating a non–Debye type of relaxation with distribution of relaxation time. The semicircular arcs gradually decrease with increasing temperature. The effect of temperature on impedance characteristics of the material becomes clearly visible in the figure. It clearly shows that the material is temperature and frequency dependant. This non ideal behavior can be related to the factors like grain boundaries, grain orientation, stress-strain phenomena and defect distribution [50].

The semicircular pattern in the impedance spectrum is representative of the electrical processes taking place in the nanoceramic samples. The equivalent electrical circuit of $Zn_{1-x}Cr_xO$ nanoceramics was carried out with ZVIEW software by fitting the experimental impedance data. It was found that the circuit model of ZnO and $Zn_{1-x}Cr_xO$ nanoceramics sample is a parallel combination of bulk resistance (R_b) and bulk capacitance (C_b) and the circuit diagram was as shown in Figure 8.The value of bulk resistance (R_b) and bulk capacitance (C_b) obtained at temperature 300-500°C was shown in Table 1 and 2 for ZnO and Cr doped samples respectively.

The impedance loss spectra has been used to evaluate the relaxation time (τ) of the electrical phenomena taking place in the material at a different temperature. The relaxation time (τ) calculated from the plot of Z'' versus log (f) by using the relation $\tau = \frac{1}{\omega} = \frac{1}{2\pi f_{max}}$ [62], where f_{max} is the frequency at which Z'' was found to be maximum. The value of τ was found to be decreasing with the rise in temperature. The relaxation time is independent of the sample geometries but dependent on the microstructure and intrinsic properties of the material. Figure 9 represents the typical variation of relaxation time (τ) with the inverse of temperature for $Zn_{1-x}Cr_xO$ in the temperature range of 300 - 400 ºC. From the figure it was observed that ZnO (x = 0) shows less relaxation time than the Cr doped sample and it increases with increase in Cr concentration. Among the doped samples x = 0.01 shows less relaxation time which has a faster response for small stimuli than others. The τ value of Cr doped ZnO sample was found to be decreased with increase in temperature which is a typical semiconductor type behavior.

Again the nature of variation of τ with temperature for all samples appear to follow the Arrhenius relation $\tau=\tau_0 \exp[-E_a/KT]$ [69]. Where τ_0 pre exponential factor, E_a = activation energy, K = Boltzmann constant and T = absolute temperature. The activation energy was evaluated from the graph of log τ Vs 1000/T shown in Figure 10. In Cr doped sample, the activation energy E_a of ZnO decreases with doping and the E_a value was found to be less than 1eV.

4 Conclusions

Cr doped ZnO ($Zn_{1-x}Cr_xO$, x = 0, 0.01, 0.02, 0.03 and 0.04) was successfully synthesized by high energy ball milling technique. Diffusion of Cr into ZnO lattice by displacing Zn up to 3% (x = 0.03) was observed after 10h of milling. But after calcination at 900 ºC 4% Cr (x = 0.04) can be soluble in ZnO. So the solubility Cr in ZnO can be extended after calcination. The structural, morphological and electrical properties of the materials are studied in detail. Particle size increases after Cr doping as obtained from XRD and FESEM result. $Zn_{1-x}Cr_xO$ ceramics have a novel NTCR effect within

temperature range 300 - 500 ºC.The impedance spectroscopy data shows a single semicircle in the high frequency region corresponding to the bulk properties of the ceramic sample. The impedance pattern suggests a decrease in bulk resistance with increase in temperature. Distributed relaxation time suggests that the relaxation in the synthesized sample is of non-Debye type and the relaxation time decreases with increase in temperature. Our observation was found to be suitable for high temperature sensor applications.

Figure:

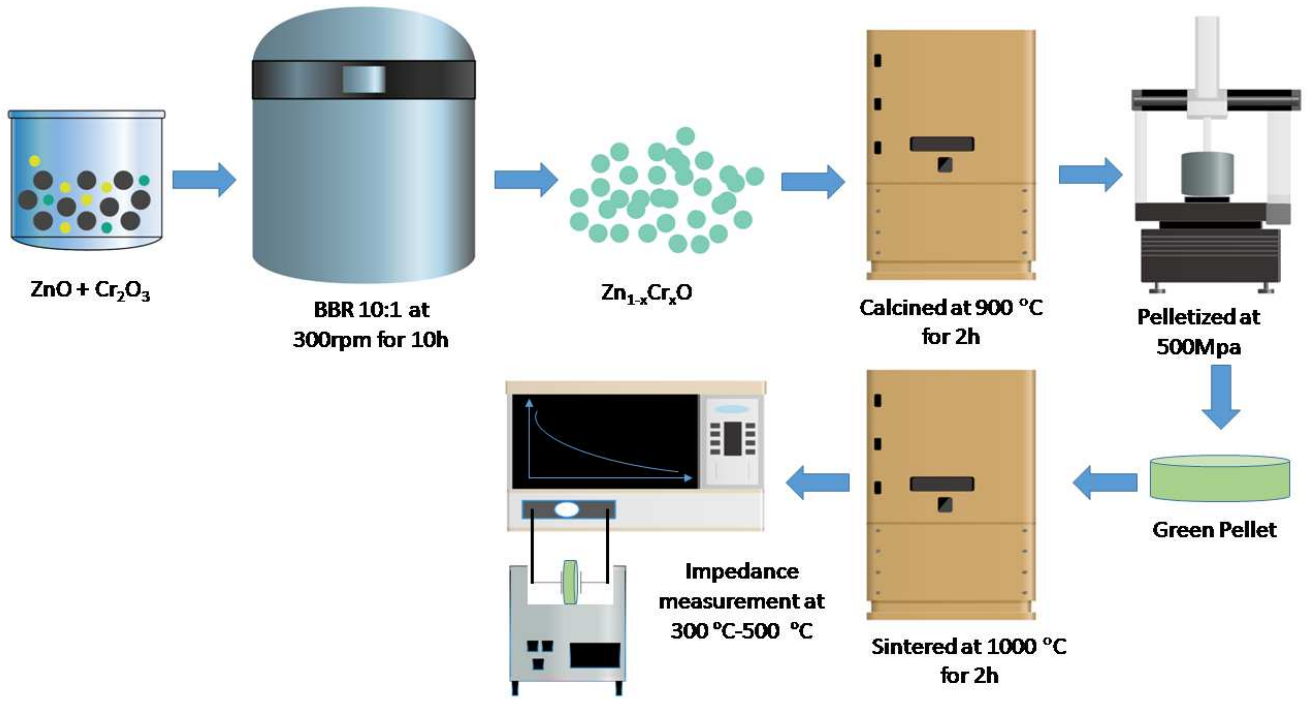

Figure 1: Schematic representation of methodology

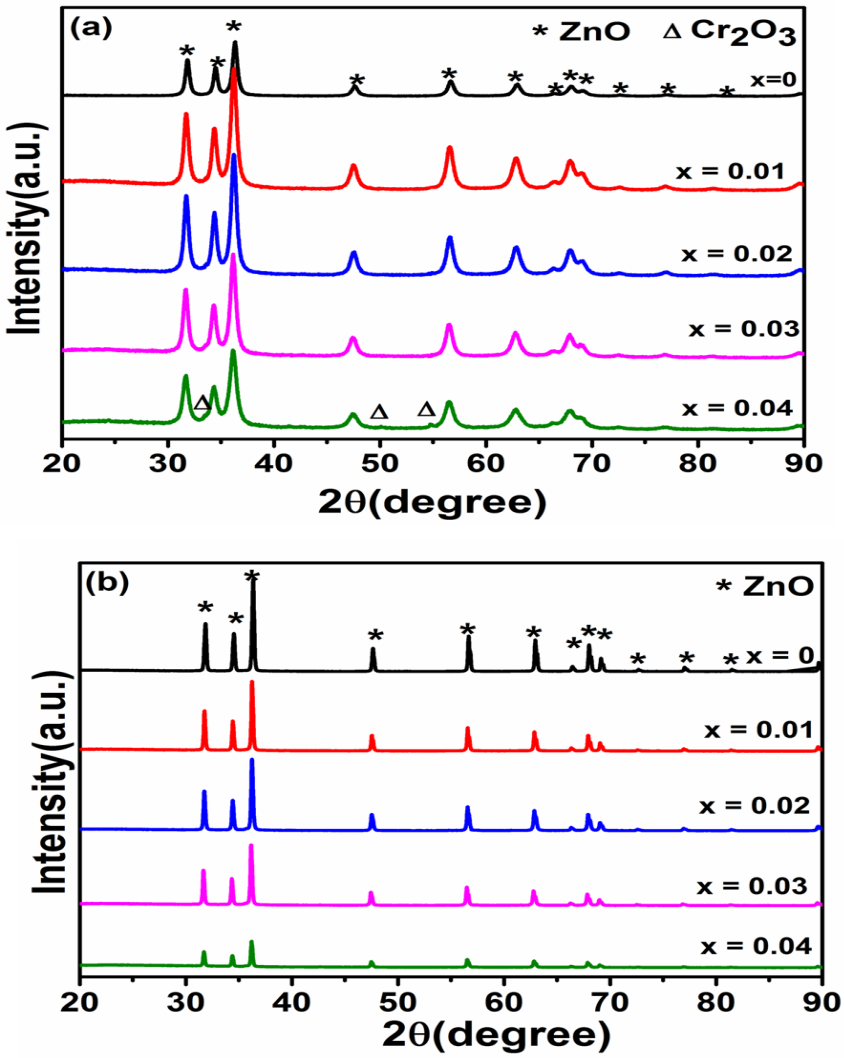

Figure 2: XRD pattern of $Zn_{1-x}Cr_xO$ (x = 0,0.01,0.02,0.03,and 0.04) nanoceramics (a) after ball milling for 10h and (b) after ball milling for 10h followed by calcination at 900 ºC for 2h.

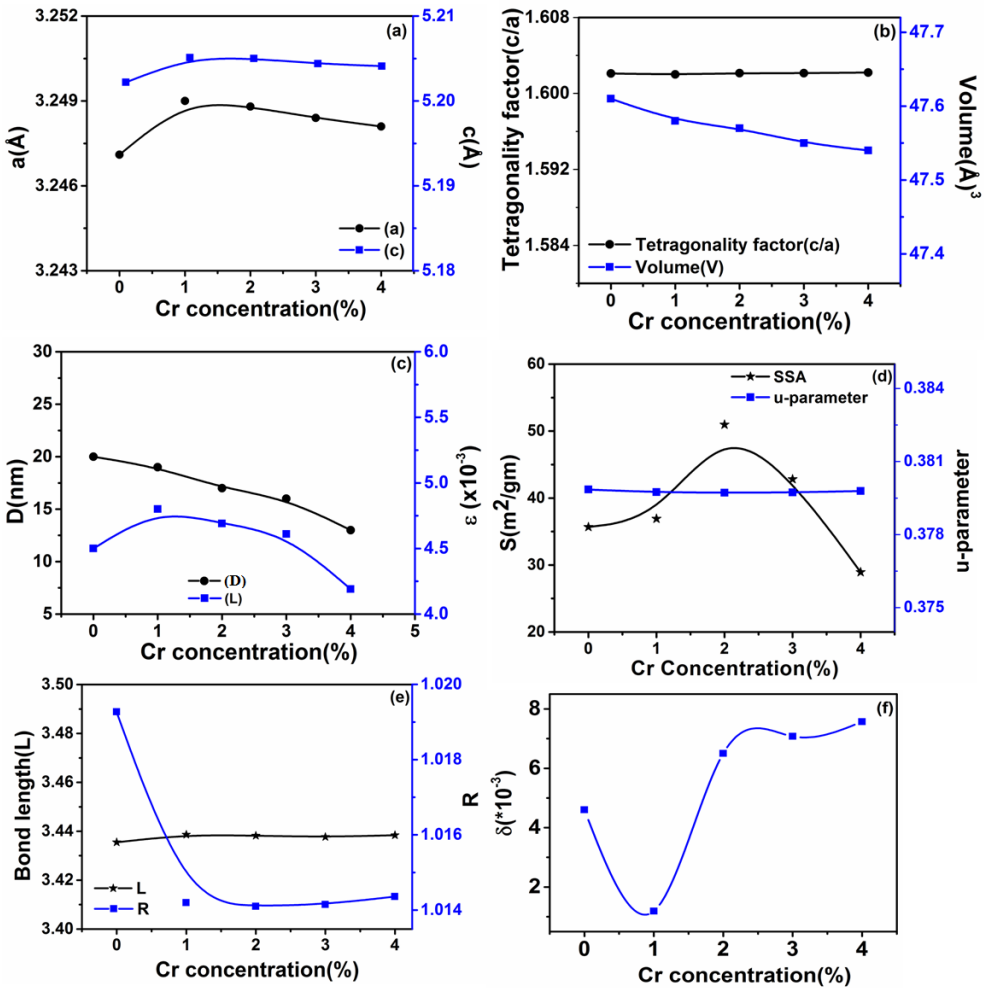

Figure 3: Variation of structural parameter with Cr concentration of 10h ball milled $Zn_{1-x}Cr_xO$ (x = 0, 0.01, 0.02, 0.03 and 0.04) nanoceramics (a) Latice pameter 'a' and 'c',(b) c/a ratio and volume (V), (c) crystallite size (D) and strain (ε), (d) specific surface area (S) and u-parameter (e) bond length (L) and crystal lattice distortion degree (R) and (f) dislocation density(δ).

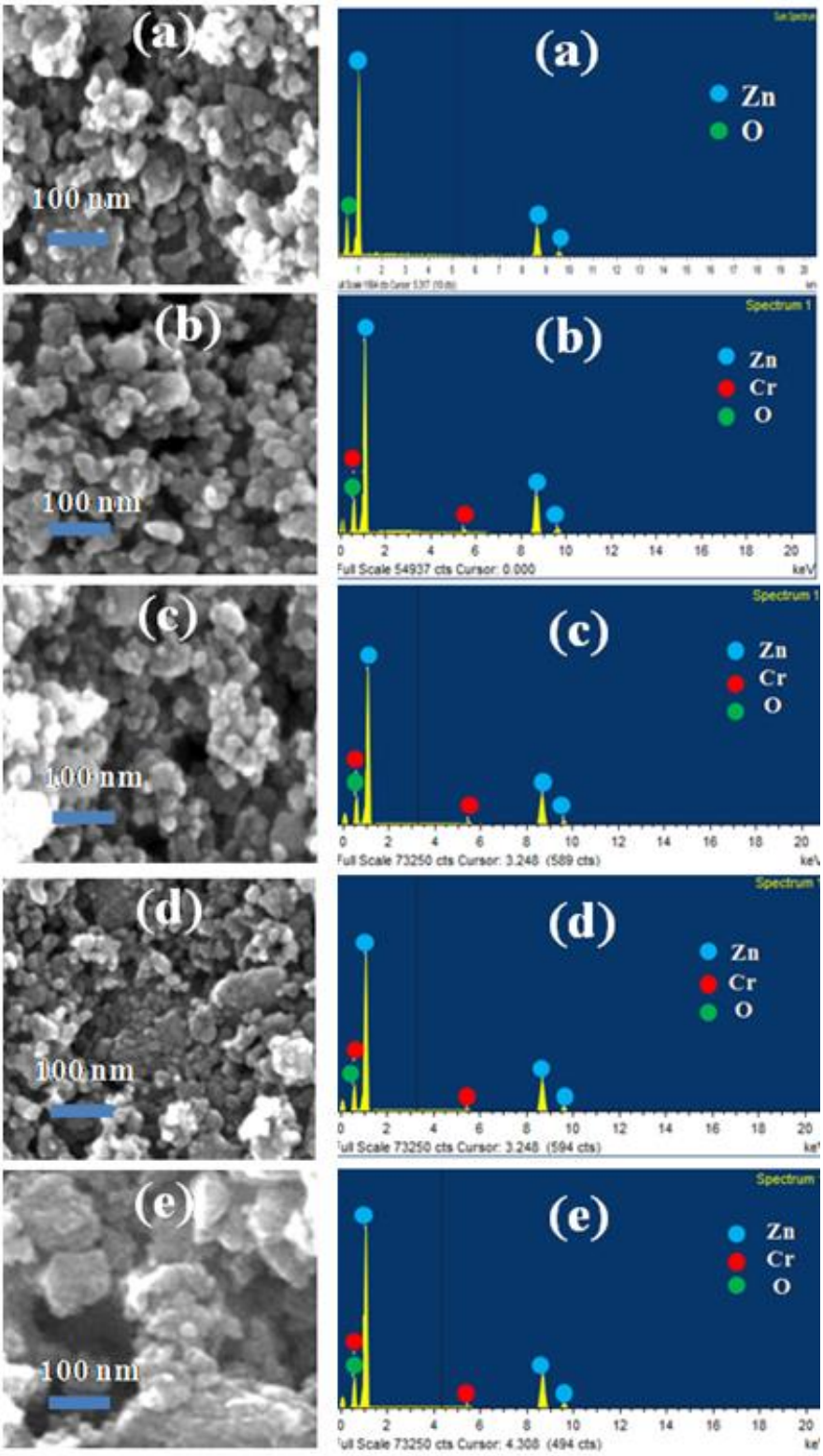

(i) **(ii)**

Figure 4: The FESEM micrograph of $Zn_{1-x}Cr_xO$ (a) x = 0, (b) x = 0.01, (c) x = 0.02, (d) x = 0.03 and (e) x = 0.04 samples (i) 10h milled uncalcined powder, and (ii) EDX of 10h milled $Zn_{1-x}Cr_xO$ samples.

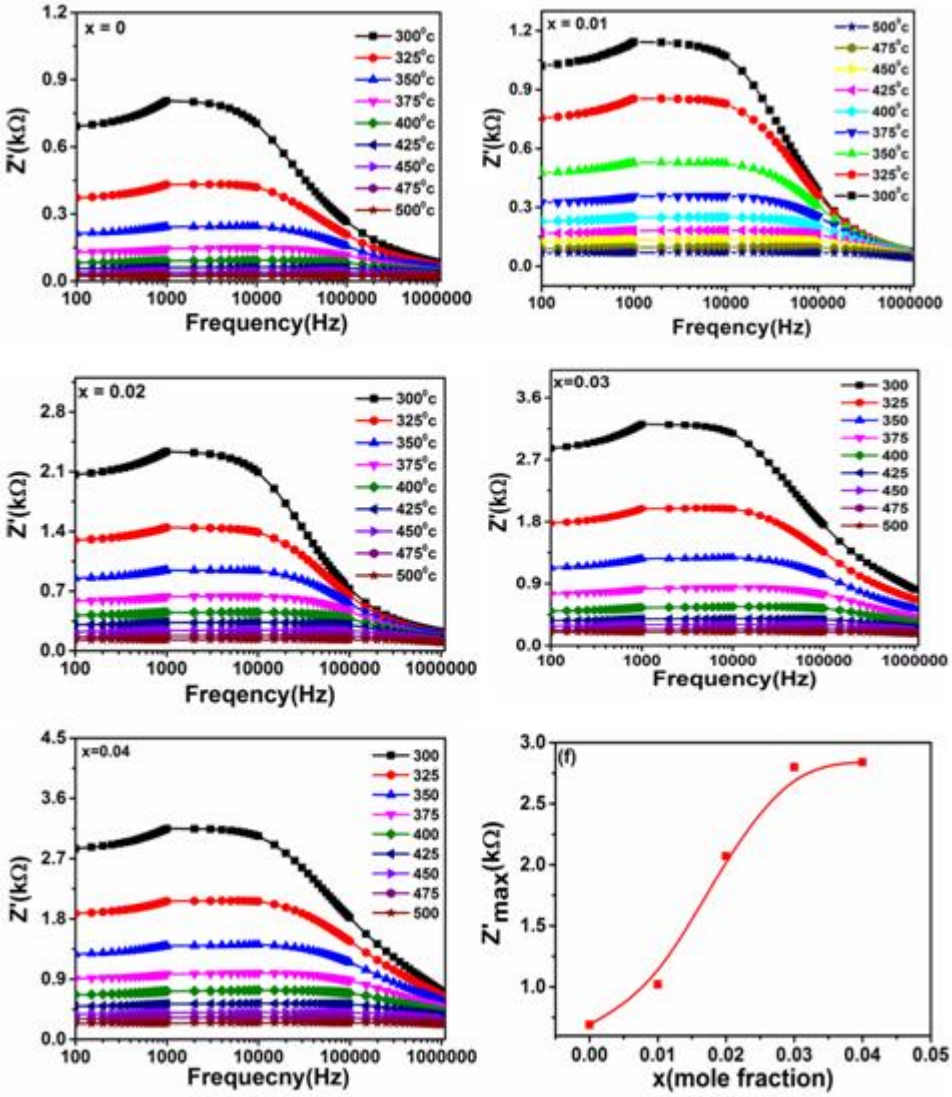

Figure 5: Variation of frequency with Z′ of the pellet sample prepared by the 10h milled powder calcinated at 900 ºC for 2h and sintered at 1000 ºC for 2h of $Zn_{1-x}Cr_xO$ (x = 0 - 0.04) nanoceramics and (f) with different Cr concentration at a particular temperature (300 ºC) and frequency 20kHz.

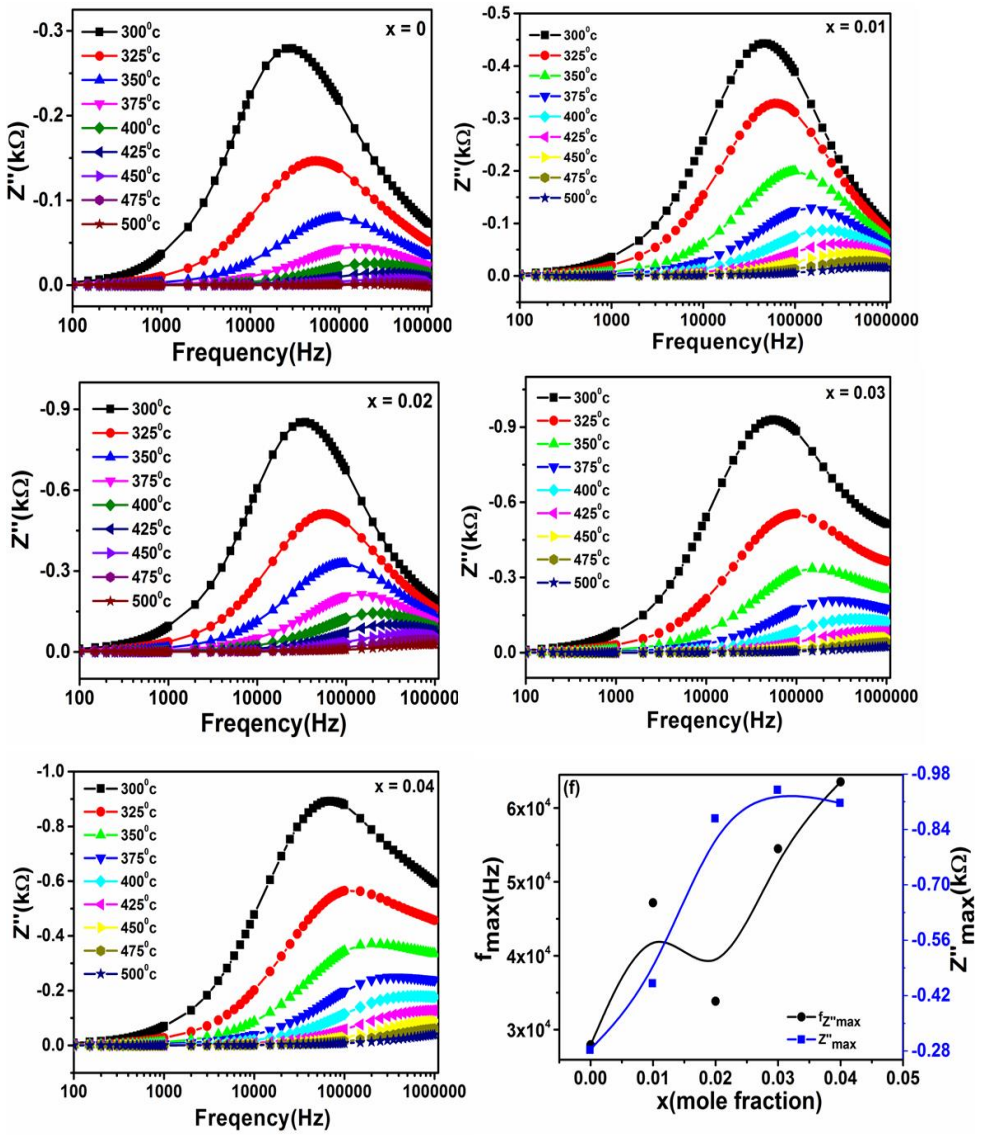

Figure 6: Variation of Z'' with frequency of $Zn_{1-x}Cr_xO$ (x = 0 - 0.04) of the pellet sample prepared from the 10h milled powder calcinated at 900 ºC for 2h with sintering at 1000 ºC for 2h and (f) Variation of f_{max} and Z''_{max} with different Cr concentration at a particular temperature (300 ºC) and frequency 20kHz.

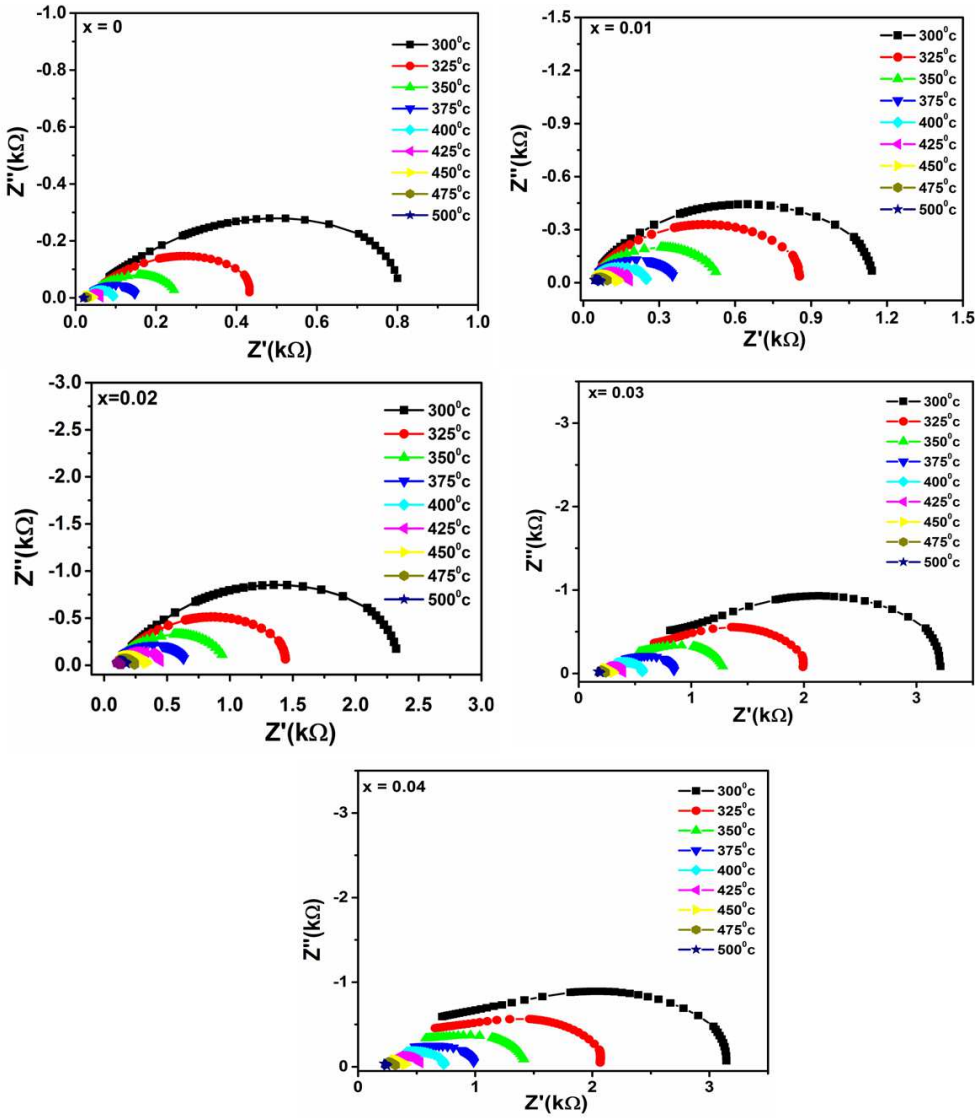

Figure 7: Z' vs Z'' plot of $Zn_{1-x}Cr_xO$ (x = 0 - 0.04) nanoceramics.

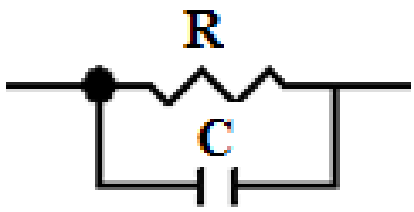

Figure 8: Corresponding circuit diagram of Cr doped ZnO nanoceramics.

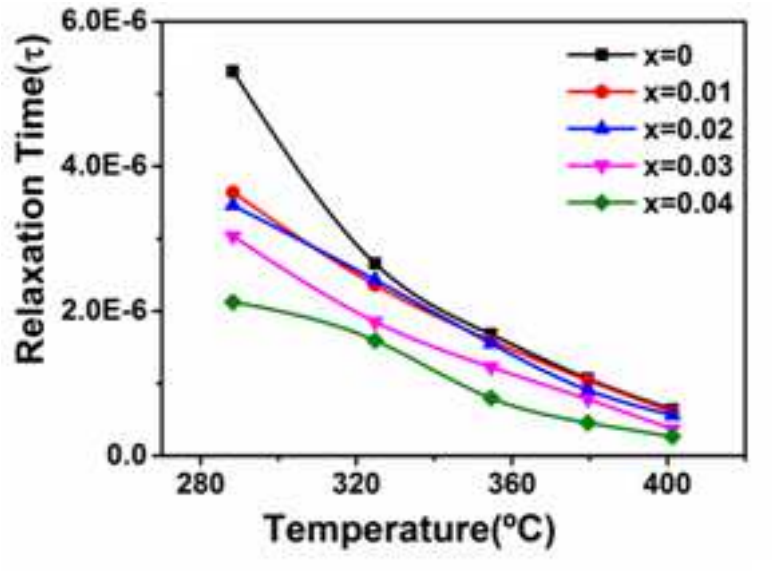

Figure 9: Variation of relaxation time (τ) with inverse of temperature of $Zn_{1-x}Cr_x$ (x = 0,0.01,0.02,0.03 and 0.04) of the pellet samples prepared using the 10h milled powders calcinated at 900 ºC for 2h and sintered at 1000 ºC for 2h.

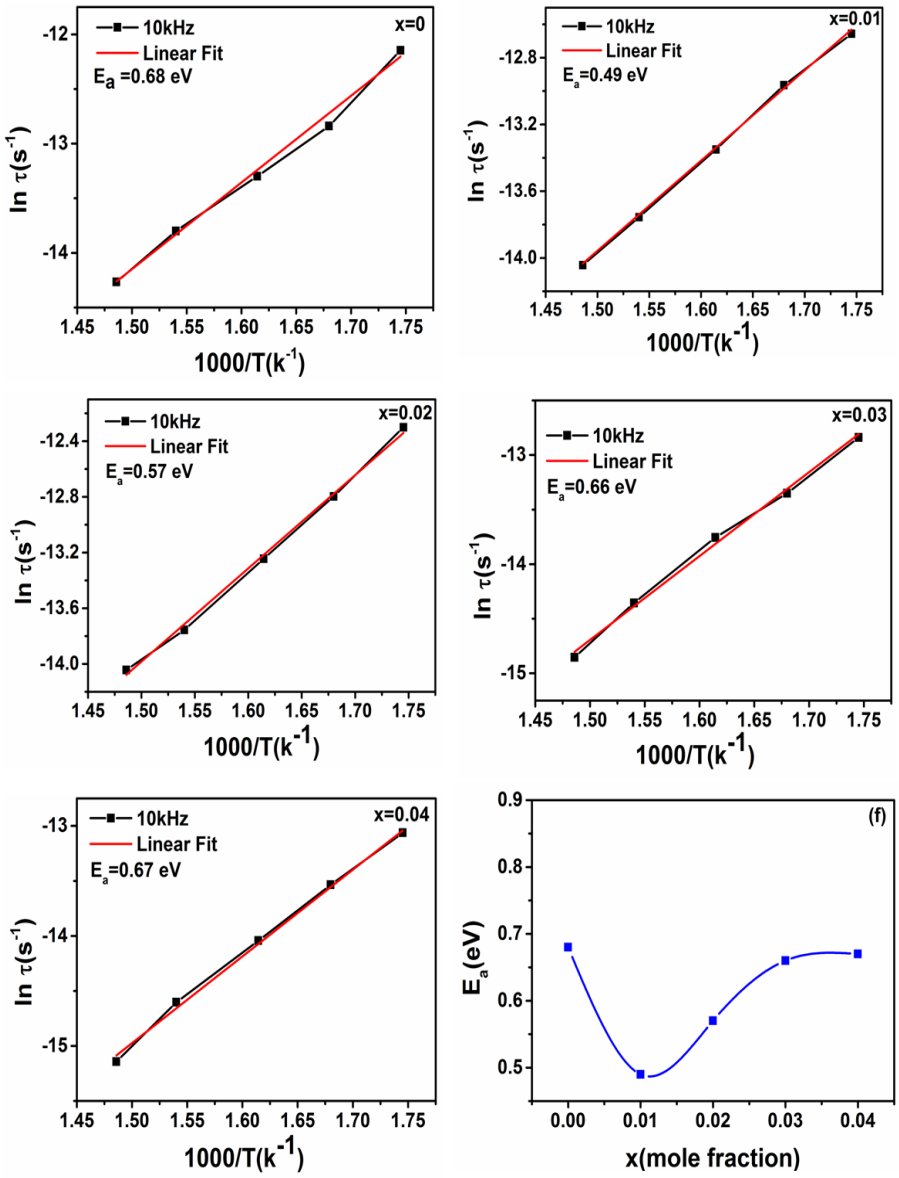

Figure 10: Variation of relaxation time (τ) with 10^3/T of $Zn_{1-x}Cr_xO$ (x = 0-0.04) nanoceramics (for impedance data) and (f) variation of E_a with Cr concentration.

Table 1: Bulk resistance (R_b) and bulk capacitance (C_b) of $Zn_{1-x}Cr_xO$ (x = 0 - 0.04) ceramics calcined at 900 °C followed by sintered at 1000 °C.

Table 5.2: Bulk resistance (R_b) and bulk capacitance (C_b) of $Zn_{1-x}Cr_xO$ (x=0-0.04) nanoceramics.

	x=0		x=0.01		x=0.02		x=0.03		x=0.04	
Temperature(°C)	R_b(kΩ)	C_b(F) (x10^{-10})	R_b(kΩ)	C_b(F) (x10^{-09})	R_b(kΩ)	C_b(F) (x10^{-10})	R_b(kΩ)	C_b(F) (x10^{-10})	R_b(kΩ)	C_b(F) (x10^{-10})
300	0.8155	5.5149	1.1374	2.7593	2.2973	1.7882	2.7941	7.5822	2.6259	0.1236
325	0.4025	5.9264	0.8369	2.7898	1.3550	1.7765	1.6081	7.565	1.5217	0.1362
350	0.2204	6.4292	0.5104	2.853	0.8810	1.7476	0.9620	8.3174	0.9577	6.8748
375	0.1186	7.6508	0.3350	2.985	0.5642	1.7695	0.5581	9.6717	0.5602	7.8904
400	0.0644	9.3535	0.2213	3.1866	0.3675	1.8414	0.3247	0.1135	0.4972	6.086
425	0.0354	1.3047	0.1510	3.4844	0.2530	1.8742	0.2192	0.1156	0.3564	5.386
450	0.0180	0.2003	0.1069	3.7173	0.1622	1.9825	0.1495	0.1242	0.2282	6.4442
475	0.0090	0.3776	0.0693	4.2112	0.1076	2.0174	0.0992	0.1334	0.1743	5.7589
500	0.0053	0.6846	0.0368	5.9377	0.0622	2.6081	0.0671	0.1375	0.1040	5.2944

Acknowledgment

The authors would like to thank the Science and Engineering Research Board (SERB), Govt. of India for providing financial support to carry out the research work of this paper for the project CRG/2019/003315.

References:

1. R. Jadhav, D. Kulkarni,V. Puri, J Mater Sci. Mater Electron. **21**,503 (2010).
2. T. Abbas, Y. Khan, M. Ahmad, S. Anwar, Solid. State. Commun. **82,** 701 (1992).
3. M. Mehedi Hassan, W. Khan, A. Azam, and A. H. Naqvi, J. Ind. Eng. Chem. **21**, 283 (2015).
4. A. Ghosh, N. Kumari, and A. Bhattacharjee, J. Nanosci. Nano Technol **2**, 485 (2014).
5. H. M. Galindo, Y. Carvajal, E. Njagi, R. A. Ristau, and S. L. Suib, Am. Chem. Soci. J. **26**, 13677 (2010).
6. M. Mittal, M. Sharma, and O. P. Pandey, Sol. Energy **110**, 386 (2014).
7. R.O. Yathisha , Y. Arthoba Nayaka, C.C. Vidyasagar, Mater. Chem. Phy **181**, 167 (2016).
8. A. Franco Jr, H.V.S. Pessoni, Physica B **506,** 145 (2017).
9. S. Goela, N. Sinhab, H. Yadava, A.bhilash J. Josepha, B.nay Kumara, Physica E **91,** 72 (2017).
10. J. H. Jun, H. Seong, K. Cho, B. M. Moon, and S. Kim, Ceram. Int. **35**, 2797 (2009).
11. M. Suchea, S. Christoulakis, K. Moschovis, N. Katsarakis, and G. Kiriakidis, Thin Solid Films **515**, 551 (2006).
12. N. Sekine, C. H. Chou, W. L. Kwan, and Y. Yang, Org. Electron. Physics, Mater. Appl. **10**, 1473 (2009).
13. S.J. Pearton, D.P. Norton, Y.W. Heo, L.C. Tien, M.P. Ivill, Y. Li, B.S. Kang, F. Ren,J. Kelly, A.F. Hebard, J. Electron. Mater.**35**, 862 (2006).
14. Y. Roig, S. Marre, T. Cardinal, and C. Aymonier, Angew. Chemie - Int. Ed. **50**, 12071 (2011).
15. Z. L. Wang and J. Song, Science. **312**, 242 (2006).
16. H. Kim, A. Piqué, J. Horwitz, H. Murata, Z. Kafafi, C. Gilmore, and D. Chrisey, Thin Solid Films **798**, 377 (2000).
17. X. Sun, H. Zhang, Y. Liu, J. Guo, Z.Cheng, J. Adva.Ceram. **5**, 329 (2016),
18. H. Zhang, B. Chen, H. Jiang, C. Wang, H. Wang, and X. Wang, Biomaterials **32**, 1906 (2011).
19. Z. Joshi , D. Dhruv, K.N. Rathod, J.H. Markna, A. Satyaprasad, A.D. Joshi, P.S. Solanki, N.A. Shah, J. Mater. Sci. Technol.**34**, 488 (2018).
20. S.H. Hsieh, J.M. Ting, Appl. Surf. Sci. **427,** 465(2018).
21. T. Das, B. K. Das, K. Parashar, R. Kumar, H. K. Choudhary, A. V. Anupama, B. Sahoo, P. K. Sahoo, and S. K. S. Parashar, J. Mater. Sci. Mater. Electron. **28**, 13587 (2017).

22. R. Beura, R. Pachaiappan, P. Thangadurai, Appl. Surf. Sci. **433**, 887(2018).
23. S. Choudhury, S. Sain, M.K. Mandal, S.K. Pradhan, A.K. Meikap, Phys. E Low-Dimensional Syst. Nanostructures. **81**, 122(2016).
24. L. Tong, W.Li, O. Shen, H. Rong, L. Gong, Materials Letters **218**, 1(2018).
25. H.H. Mohamed Journal of Photochemistry and Photobiology A: Chemistry, S1010603017312625 (2017).
26. B. K. Das, T. Das, K. Parashar, A. Thirumurugan, and S. K. S. Parashar, J. Mater. Sci. Mater. Electron. **28**, 15127 (2017).
27. A.A. Othman , Manar A. Ali , E.M.M. Ibrahim , M.A. Osman J. Alloys Compd. **683**, 399 (2016).
28. H. Ohno, Science **281**, 951 (1998).
29. G. A. Prinz, Science **282**, 1660 (1998).
30. M.H. Huang, S. Mao, H. Feick, H. Yan, Y. Wu, H. Kind, E. Weber, R. Russo, P. Yang Science **292**, 1897(2001).
31. J. M. D. Coey, M. Venkatesan, and C. B. Fitzgerald, Nat. Mater. **4**, 173 (2005).
32. A. Ishizumi and Y. Kanemitsu, Appl. Phys. Lett. **86**, 1 (2005).
33. Z. Zhou, T. Komori, M. Yoshino, M. Morinaga, N. Matsunami, A. Koizumi, and Y. Takeda, Appl. Phys. Lett. **86**, 0 (2005).
34. J. M. Sun, W. Skorupa, T. Dekorsy, M. Helm, L. Rebohle, and T. Gebel, Appl. Phys. Lett. **85**, 3387 (2004).
35. K. Potzger, S. Zhou, F. Eichhorn, M. Helm, W. Skorupa, A. Mücklich, J. Fassbender, T. Herrmannsdörfer, and A. Bianchi, J. Appl. Phys. **99**, (2006).
36. S. H. Deng, M. Y. Duan, M. Xu, and L. He, Phys. B Condens. Matter **406**, 2314 (2011).
37. J. Hays, K. M. Reddy, N. Y. Graces, M. H. Engelhard, V. Shutthanandan, M. Luo, C. Xu, N. C. Giles, C. Wang, S. Thevuthasan, and A. Punnoose, J. Phys. Condens. Matter **19**, (2007).
38. M. A. Ciciliati, M. F. Silva, D. M. Fernandes, M. A. C. De Melo, A. A. W. Hechenleitner, and E. A. G. Pineda, Mater. Lett. **159**, 84 (2015).
39. T. Das, B. K. Das, K. Parashar, and S. K. S. Parashar, Acta Phys. Pol. A **130**, 1358 (2016)
40. X. Yan and G. Xu, Phys. B Condens. Matter **404**, 2377 (2009).
41. X. Li, Y. Luo, and X. Liu, Adv. Mater. Sci. Eng. **2009**, 0 (2009).
42. G. Ray , S.anjay Godara, M.K. Gupta, B. Kumar, Mater. Res. Bull. **59** 267(2014).
43. M. H. Bezerra Junior, T. O. Abreu, F. F. do Carmo, J. E. V. de Morais, R. G. M. Oliveira, M. A. S. Silva, H. D. de Andrade, I. S. Queiroz Junior, J. C. M. Mota, A. S. B. Sombra, J Mater Sci: Mater Electron (2021)

44. M. Pollak, T.H. Geballe, Phys. Rev. **122**, 1742(1961).
45. P. Norouzzadeh, Kh. Mabhouti, M. M. Golzan , R. Naderali, J Mater Sci: Mater Electron **31,** 7335–7347 (2020)
46. N. Kılınc¸L. Arda, S. Oztürk, Z.Z. Oztürk, Cryst. Res. Technol. **45**, 529(2010).
47. M. Chaari, A. Matoussi, Physica B **407**, 3441(2012).
48. M. Ashokkumar, S. Muthukumaran, Opt. Mater.**37**, 671(2014).
49. S. Dey, S.K. Dey, B. Ghosh , V.R. Reddy and S. Kumar, Chem. Phys.**138**, 833(2013).
50. B. K Das, T. Das, K. Parashar and S K S Parashar, Appl. Sci. and Adv. Mater. Int. **2**, 69 (2016).
51. S. Kumar, N. Tiwari, S.N. Jha, S. Chatterjee, D. Bhattacharyya, A.K. Ghosh, RSC Adv. **6**, 107816 (2016).
52. R. Bhargava, P.K. Sharma, S. Kumar, A.C. Pandey, N. Kumar, J. Solid State Chem. **183**, 1400(2010).
53. M. Mehedi Hassan, W. Khan, A. Azam, A.H. Naqvi, J. Ind. Eng. Chem. **21,** 283(2015).
54. K. Sebayang, S. Taslima, M. Ginting, P. Sebayang, N. Bukit, Chem. Mater. Res. **9**, 30(2017).
55. S.S. Sartiman, N.F. Djaja, R. Saleh, Mater. Sci. Appl., **2013,** 528(2013).
56. V.D. Mote, World J. Condens. Matter Phys. **2**, 208(2012).
57. S. Suwanboon, P. Amornpitoksuk, P. Bangrak, Ceram. Int. **37**, 333(2011).
58. O. Altintaş Yildirim, C. Ceram. Int.**42**, 3229(2015).
59. N.F. Djaja, A. Noorhidayati, R. Saleh, AIP Conf. Proc. **1719**, (2016).
60. I. Esparza, M. Paredes, R. Martinez, A. Gaona-Couto, G. Sanchez-Loredo, L.M. Flores-Velez, O. Dominguez, Mater. Sci. Appl. **2**, 1584(2011).
61. O. Gürbüz, M. Okutan, Appl. Surf. Sci. **387**, 1211(2016).
62. U. Ozgür, Y.I. Alivov, C. Liu, A. Teke, M.A. Reshchikov, S. Doğan, V. Avruti n, S.J. Cho, H. Morkǫ, J. Appl. Phys. **98**, 1–103(2005).
63. T. Pandiyarajan, B. Karthikeyan, J. Nanoparticle Res. **14**, 647(2012).
64. R. John, R. John, R. Rajakumari, Nano Micro lett. **2**, 65(2016).
65. W. Zhang, Z. Liu, Z. Liu, J. Zhao, Appl. Surf. Sci. **258**, 6103 (2012).
66. X. Chu, S. Zhou, Y. Dong, W. Sun, X. Ge, Mater. Chem. Phys. **131**, 27(2011).
67. K. Vojisavljević, M. Ćepanović, T. Srećković, M. Grujić-Brojin, Z. Branković, G. Branković, J. Phys. Condens. Matter. **20**, 475202(2008).
68. S. Suwanboon, P. Amornpitoksuk, Ceram.Int.**37**, 3515 (2011).
69. T. Das, B.K. Das, K. Parashar, R. Kumar, H.K. Choudhary, A. V. Anupama, B. Sahoo, P.K. Sahoo, S.K.S. Parashar, Effect of Sr-doping on sinterability, morphology, structure,

photocatalytic activity and AC conductivity of ZnO ceramics, J. Mater. Sci. Mater. Electron. **28** (2017) 13587–13595.

Figures

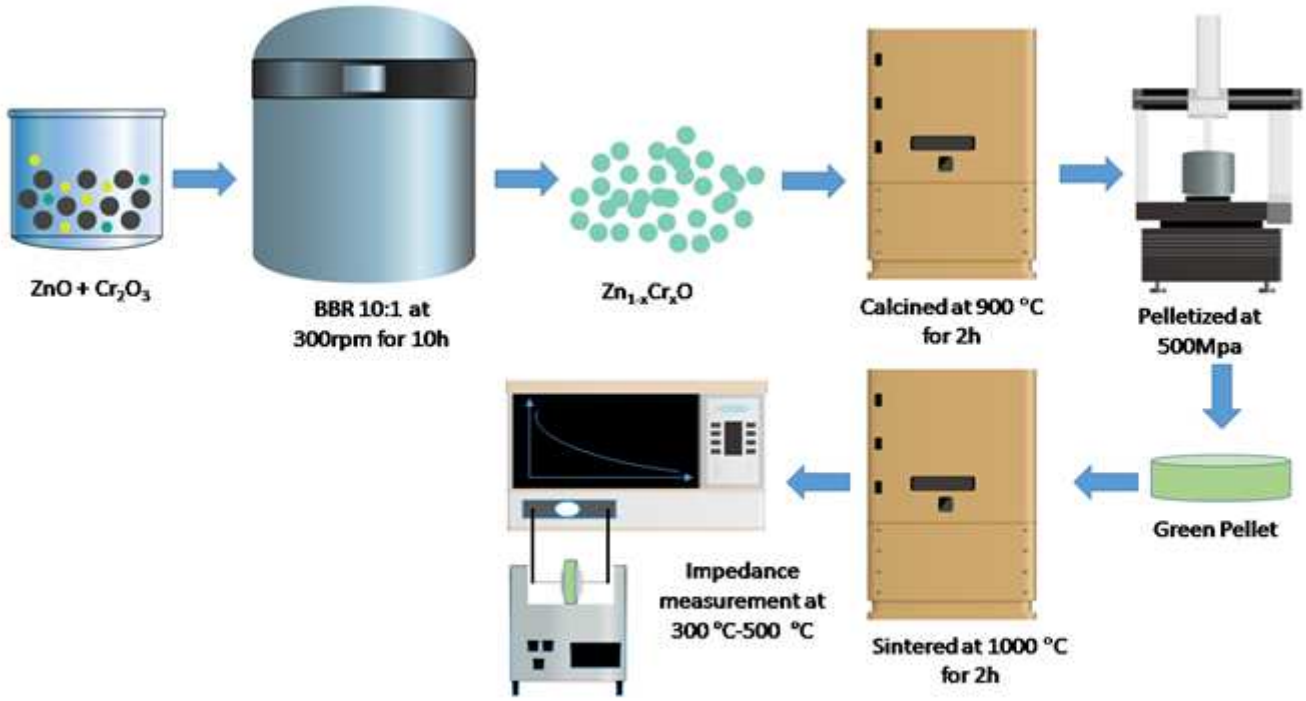

Figure 1

Figure 1

Schematic representation of methodology

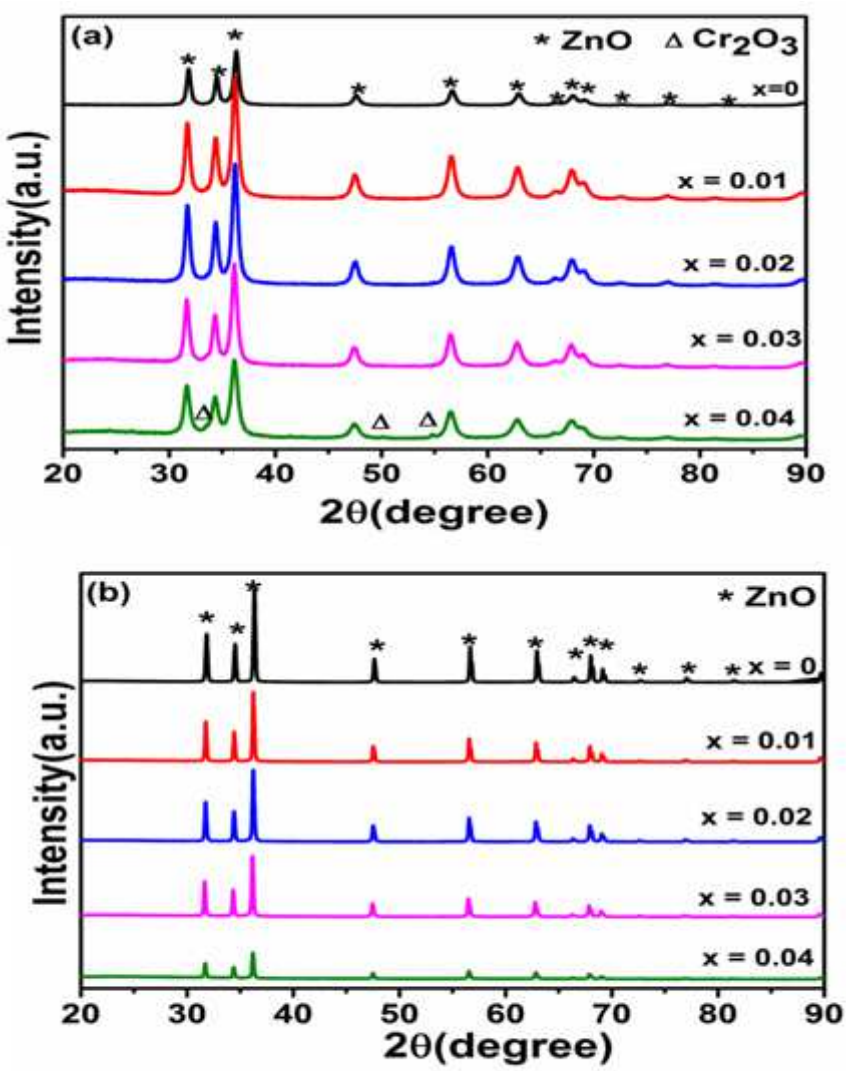

Figure 2

Figure 2

XRD pattern of Zn1-xCrxO (x = 0,0.01,0.02,0.03,and 0.04) nanoceramics (a) after ball milling for 10h and (b) after ball milling for 10h followed by calcination at 900 ºC for 2h.

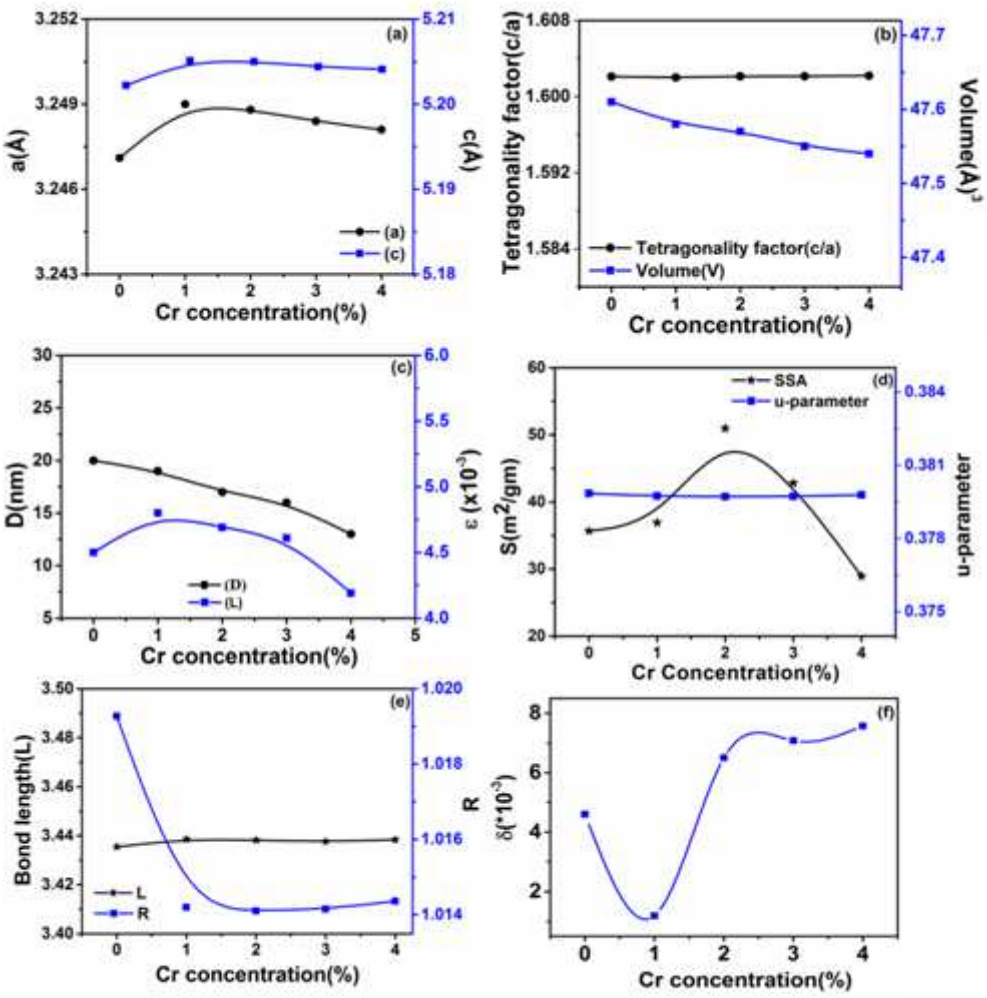

Figure 3

Figure 3

Variation of structural parameter with Cr concentration of 10h ball milled Zn1-xCrxO (x = 0, 0.01, 0.02, 0.03 and 0.04) nanoceramics (a) Latice pameter 'a' and 'c',(b) c/a ratio and volume (V), (c) crystallite size (D) and strain (ε), (d) specific surface area (S) and u-parameter (e) bond length (L) and crystal lattice distortion degree (R) and (f) dislocation density(δ).

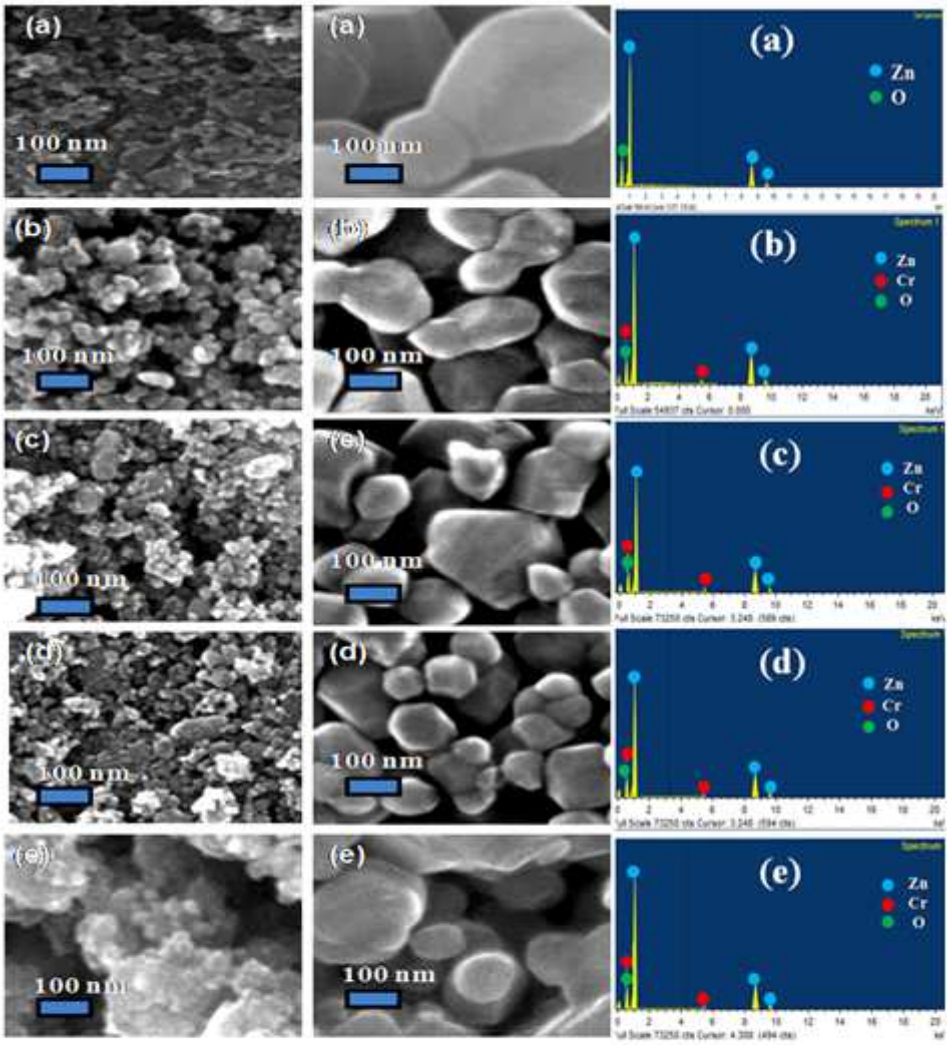

Figure 4

Figure 4

The FESEM micrograph of Zn1-xCrxO (a) x = 0, (b) x = 0.01, (c) x = 0.02, (d) x = 0.03 and (e) x = 0.04 samples (i) 10h milled uncalcined powder, and (ii) EDX of 10h milled Zn1-xCrxO samples.

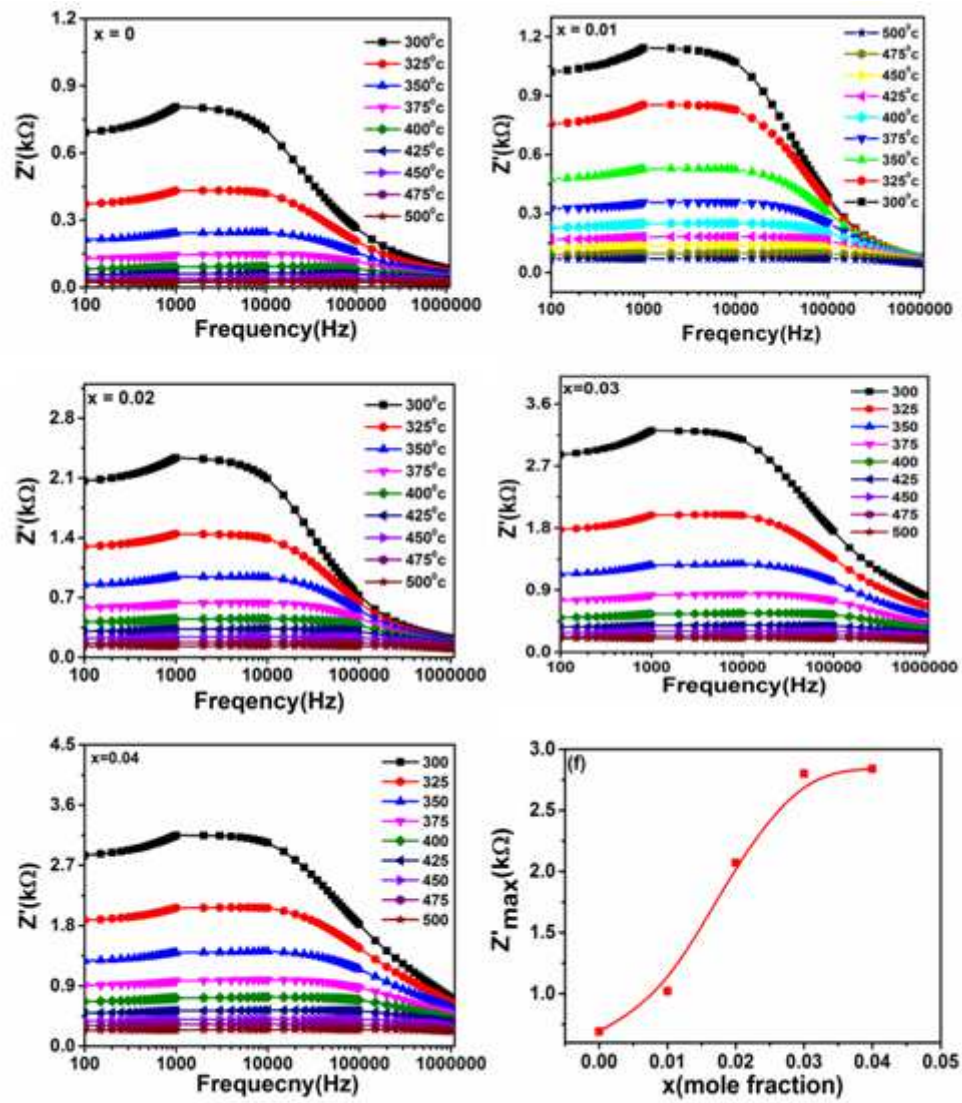

Figure 5

Figure 5

Variation of frequency with Z of the pellet sample prepared by the 10h milled powder calcinated at 900 ºC for 2h and sintered at 1000 ºC for 2h of Zn1-xCrxO (x = 0 - 0.04) nanoceramics and (f) with different Cr concentration at a particular temperature (300 ºC) and frequency 20kHz.

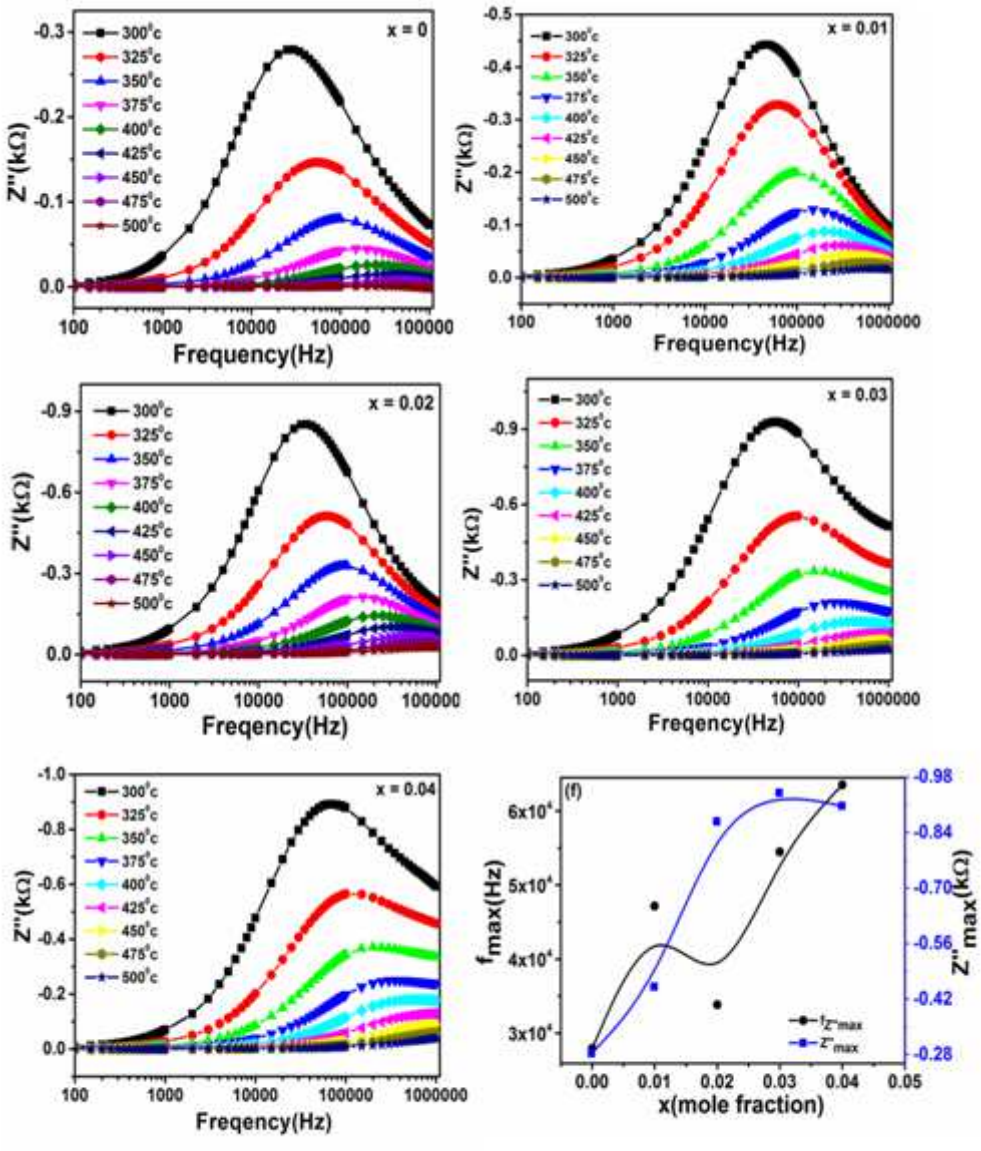

Figure 6

Figure 6

Variation of Z" with frequency of Zn1-xCrxO (x = 0 - 0.04) of the pellet sample prepared from the 10h milled powder calcinated at 900 ºC for 2h with sintering at 1000 ºC for 2h and (f) Variation of fmax and Z"max with different Cr concentration at a particular temperature (300 ºC) and frequency 20kHz.

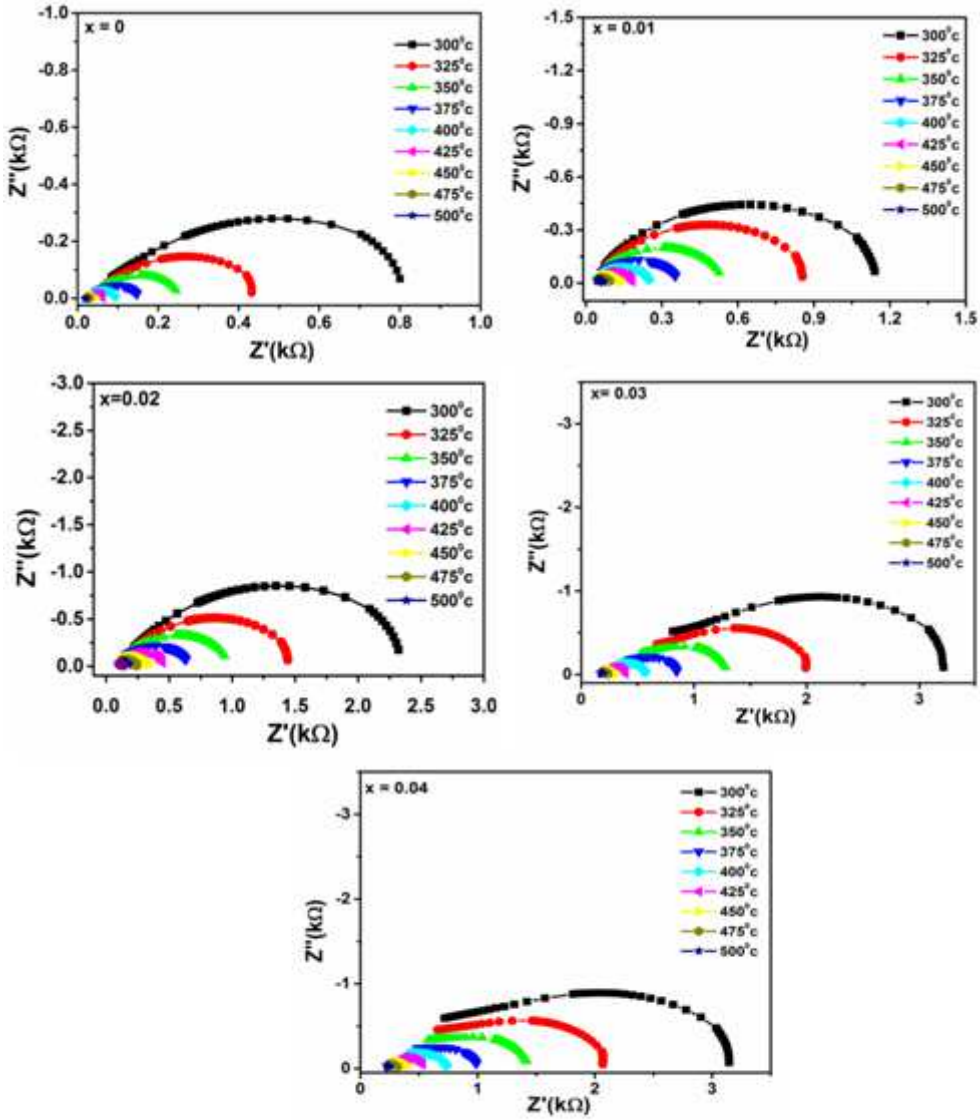

Figure 7

Figure 7

Z' vs Z" plot of Zn1-xCrxO (x = 0 - 0.04) nanoceramics.

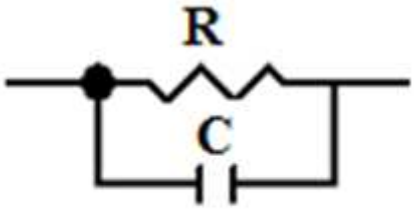

Figure 8

Figure 8

Corresponding circuit diagram of Cr doped ZnO nanoceramics.

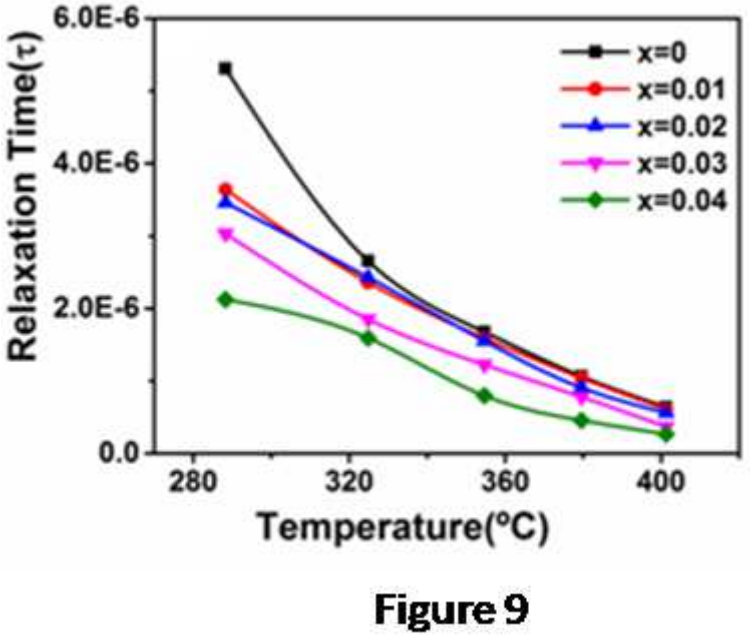

Figure 9

Variation of relaxation time (□) with inverse of temperature of Zn1-xCrx (x = 0,0.01,0.02,0.03 and 0.04) of the pellet samples prepared using the 10h milled powders calcinated at 900 ºC for 2h and sintered at 1000 ºC for 2h.

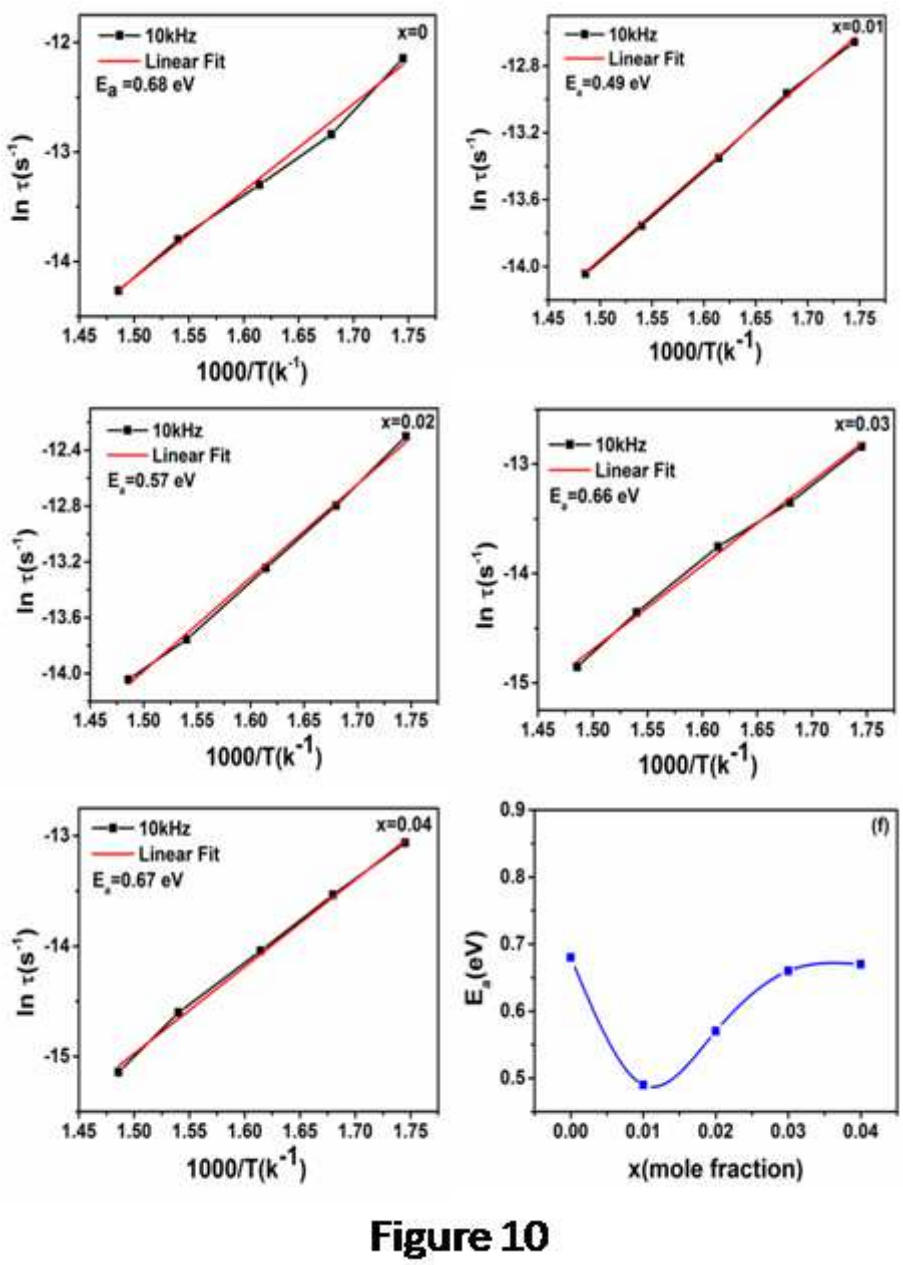

Figure 10

Figure 10

Variation of relaxation time ( ) with 103/T of Zn1-xCrxO (x = 0-0.04) nanoceramics (for impedance data) and (f) variation of Ea with Cr concentration.